Investigation of the Molecular Surface Coating on the Stability of Insulating Magnetic Oils

7 AUTHORS, INCLUDING:

Wesley Renato Viali
São Paulo State University
11 PUBLICATIONS **73** CITATIONS

Gustavo B. Alcantara
University of Brasília
12 PUBLICATIONS **123** CITATIONS

Patrícia Sartoratto
Universidade Federal de Goiás
24 PUBLICATIONS **199** CITATIONS

Ewa Mosiniewicz-Szablewska
Polish Academy of Sciences
34 PUBLICATIONS **307** CITATIONS

Investigation of the Molecular Surface Coating on the Stability of Insulating Magnetic Oils

**Wesley R. Viali,[†] Gustavo B. Alcantara,[‡] Patricia P. C. Sartoratto,[†] Maria A. G. Soler,*,[‡]
Ewa Mosiniewicz-Szablewska,[§] Bartlomiej Andrzejewski,[||] and Paulo C. Morais[‡]**

*Instituto de Quimica, Universidade Federal de Goias, Goiania GO 74001-970, Brazil, Instituto de Fisica,
Universidade de Brasilia, Brasilia DF 70910-900, Brazil, Institute of Physics, Polish Academy of Sciences,
Al. Lotnikow 32/46, 02-668 Warsaw, Poland, and Institute of Molecular Physics, Polish Academy of Sciences,
Smoluchowskiego 17, 60-179 Poznan, Poland*

Surface functionalization of a series of nanosized iron oxide particles (average diameter around 6 nm) with oleic acid was realized in this study. The aim is to suspend the surface-functionalized nanoparticulated materials in insulating mineral oil and evaluate their colloidal stability as a function of time. Nanoparticulated samples presenting stoichiometry close to maghemite were obtained by oxidation of a freshly precipitated magnetite sample. Systematic variations observed in the Fe^{3+}/Fe^{2+} ratio, average particle size, and lattice constant were attributed to differences in oxidation route and oxidation condition employed. Morphological, compositional, thermal, optical and magnetic characterization techniques were used in the investigation of native (P, PN1, PN2, POX1, POX3, and POX7) and surface-functionalized (POA, PN1OA, PN2OA, POX1OA, POX3OA, and POX7OA) samples. While suspending the oleic-acid-coated nanosized iron oxide particles in insulating mineral oil, the best colloidal stability was achieved at the oxidation profile of $Fe^{3+}/Fe^{2+} = 40$ (5.9 nm average core diameter), leading to a surface grafting coefficient of about 75% of a full monolayer coating of chemisorbed species only and resulting in the smallest observed hydrodynamic radius (8.1 nm). Within the range of our investigation, our findings reveal the characteristics and the chemical protocol used to produce a magnetic fluid sample embodying long-term colloidal stability, thus representing a very much promising material for application as a refrigerating fluid in power transformers and related devices.

Introduction

Over the past two decades, nanosized materials, for instance, superparamagnetic iron oxide (SPIO), have received a great deal of attention focusing on topics as different as insulating magnetic oils for transformers[1−4] and drug delivery systems for cancer therapy,[5] particularly due to the unusual and enhanced properties of such materials,[6,7] opening up perspectives for a wide variety of industrial and medical applications.[8−10] Nanosized particles consisting of iron-based cubic ferrites, more specifically, magnetite (Fe_3O_4) and maghemite (γ-Fe_2O_3), represent typical SPIO materials, embodying improved chemical stability and enhanced biological compatibility. SPIO-based magnetic fluids (MFs) have long been used in several industrial applications and more recently exploited as a very promising material platform for biomedical applications[11] while providing simple routes for incorporation of nanosized magnetic particles in different hosting templates.[12−15] However, each particular application demands very specific characteristics of the SPIO-based material and the corresponding surface-functionalization, taking into account the chemical and structural stability of the nanoparticle core as well as the physicochemical and biological properties of the molecular layer adsorbed onto the nanoparticle surface, the latter playing a key role on the MF colloidal stability. Two basic mechanisms have been used to promote colloidal stability while preparing magnetic fluids: the steric and the electrostatic repulsion mechanisms aimed to overcome van der Waals and magnetic dipole attractions.[16] Stable MF samples can be prepared using several routes.[17] An approach for the production of nonaqueous high-quality MF samples is the thermal decomposition of iron precursors in the presence of hot organic surfactants.[18] Willis et al. reported the synthesis of monodisperse maghemite (diameter around 11 nm) from tri-octylamine, oleic acid, and $Fe(CO)_5$ using a high-temperature decomposition reaction.[19] The oleic acid (OA) promotes the nanoparticle surface passivation and renders the nanosized particle stable in a variety of organic media. By monitoring the surfactant chemical structure during the nanoparticle synthesis, the authors found that the OA coating is chemically transformed during the high-temperature synthesis process, leading the formation of high-quality nanosized maghemite particles.[19] In another approach, Pascal et al. developed an electrochemical synthesis route for nanosized maghemite in organic medium.[20] The authors claim that the particle diameter could be controlled between 3 and 8 nm by adjusting the imposed current density while adsorption of long-chain tetraalkylammonium salts prevent particle aggregation in organic media.[20] Sahoo et al. have produced surface-coated magnetite particles (6−8 nm average diameter) using different surfactants (OA, lauric acid, dodecyl phosphonate, hexadecyl phosphonate, and dihexadecyl phosphonate) in order to stabilize the nanosized particles and disperse them in organic solvents.[21] In contrast, water-based MF samples can be produced by surface dressing the nanosized particle using molecular coatings presenting ionizable functional groups facing the bulk solvent, thus adding an extra component to the colloidal stability of the MF sample through the electrostatic repulsion. Among the huge variety of chemical routes used to synthesize

* To whom correspondence should be addressed. Tel: +55-61-3307-2900. Fax: +55-61-3307-2363. E-mail: soler@unb.br.
† Universidade Federal de Goias.
‡ Universidade de Brasilia.
§ Institute of Physics, Polish Academy of Sciences.
|| Institute of Molecular Physics, Polish Academy of Sciences.

nanosized particles,[22,23] the coprecipitation via alkaline hydrolysis of transition-metal ions in aqueous media[24−27] has been widely used due to their technical simplicity, higher yield, and facility for scaling up. Detailed studies have been developed to understand the influence of the synthesis parameters governing the coprecipitation reaction and the role they play on the as-produced particle characteristics (such as core structure, size and shape profile, and chemical and structural stability). Jolivet et al. investigated the influence of the Fe^{2+}/Fe^{3+} ratio on the mechanism of iron oxide formation in alkaline medium.[28] Gnanaprakash et al. reported the effect of digestion time and alkali addition rate on the size and magnetic properties of precipitated magnetite nanoparticles.[29] Using coprecipitation, Morais et al. have modulated the core size of cobalt ferrite nanoparticles by controlling the stirring speed of the reaction medium.[27] Indeed, the efficacy of grafting molecules at the SPIO surface for further encapsulation in a hosting template or for direct application is a key technical aspect and requires a full understanding of the consequences of the surface modification upon both the nanoparticle core and the nanoparticle shell in regard to their physical and chemical properties.

The power transformers are important devices within any electrical system and are involved in the processes of transmission and distribution of electrical energy. The most common transformer is the one containing its internal parts immersed in insulating oil, which is also responsible for the device refrigeration during its operation. The performance of this equipment is associated, among other effects, with the insulating and refrigerating characteristics of the insulating oil. The presence of nanosized magnetic particles within the oil phase increases the dielectric constant of the fluid and makes possible the size reduction of the equipment and/or the device operation at higher voltages.[1] Furthermore, the device refrigeration efficiency can be enhanced by using insulating magnetic oils once the effective heat transfer process is now enhanced due to thermomagnetic convection arising from the interaction between the nanoparticle magnetic moment and the magnetic field gradient within the device. Theoretical analysis suggested that the heat flux can increase by about 20% while using magnetic oil containing a 1% volume fraction of SPIO-based nanoparticles.[4] Although the subject has been already reported in the literature,[1−4,30−40] the very promising industrial application of insulating magnetic oils for transformers, expected to provide device extended life at higher efficiency operation profiles while reducing the risk of accidents, is at its infancy.

In regard to the production of insulating magnetic oils for transformers,[1−4] the MF samples used to fabricate them demand dilution as high as 3 to 4 orders of magnitude and, therefore, require enhanced colloidal stability while operating at elevated temperatures, at high voltages, and for long periods of time. To achieve the required higher MF colloidal stability, fine control of the SPIO molecular surface coating is required. Considering that preparation of stable insulating magnetic oil for transformer applications is a complex process, involving multiple steps, not yet technically dominated to reach the market, it is important to build a deeper understanding of the relation between the synthetic route and the stability of both the core nanoparticle and the molecular surface coating. With this purpose in mind, the present study reports on the preparation and characterization of insulating magnetic oils based on OA-coated maghemite nanoparticles. The maghemite nanoparticle was obtained via two different routes of oxidation of previously synthesized magnetite nanoparticle, surface-coated with OA in a subsequent step, suspended as diluted MF samples and finally

used as a model system for long-term colloidal stability investigations. Multiple experimental techniques, namely, X-ray diffraction (XRD), transmission electron microscopy (TEM), infrared (IR) spectroscopy, thermogravimetric analysis (TGA), dynamic light scattering (DLS), Raman spectroscopy (RS), and magnetic measurements were employed in a complementary way to draw a picture linking the sample's preparation and their physical and chemical properties.

Experimental Section

Magnetic Fluid Preparation. The nanosized magnetite (Fe_3O_4) precursor was synthesized by coprecipitating Fe^{2+} and Fe^{3+} in alkaline medium. $FeCl_2 \cdot 4H_2O$ (375 mL, 0.30 mol L^{-1}) and 375 mL of $FeCl_3 \cdot 6H_2O$ (0.60 mol L^{-1}) were mixed, and the resulting solution was slowly added to 750 mL of NaOH (1.5 mol L^{-1}) under mechanical stirring (2000 rpm) at room temperature. The as-precipitated black material (solid magnetite) was isolated by centrifugation and washed with distilled water until the supernatant reached pH 7. Portions (five) of the solid black precursor (sample P) were then used for further oxidation following two different routes, both aiming to produce nanosized maghemite: (i) by hydrothermal treatment (HT treatment) of the solid precursor with ferric nitrate/nitric acid solution,[26] originating samples PN1 and PN2, or (ii) by bubbling O_2 gas (BO treatment) through acidic (HCl) aqueous suspensions containing the solid precursor,[25] producing samples POX1, POX3, and POX7. Sample PN1 was obtained using 12 g of the solid precursor added to the solution containing 40 mL of HNO_3 (2.0 mol L^{-1}) and 60 mL of $Fe(NO_3)_3$ (0.70 mol L^{-1}) under stirring, heated at 97 °C for 1 h. After cooling, sample PN1 was isolated by centrifugation and washed several times with acetone/water solution. Sample PN2 was obtained similarly, but using an aqueous solution of $Fe(NO_3)_3$ (1.4 mol L^{-1}) instead. Sample POX1 was obtained using 12 g of the solid precursor dispersed in 100 mL of water adjusted to pH 3.5 using HCl aqueous solution at 3.0 mol L^{-1}. The suspension was stirred and heated at 97 °C while O_2 gas was bubbled throughout the solution during 1 h. After cooling, sample POX1 was isolated and washed several times with acetone/water. Samples POX3 and POX7 were obtained similarly, except that O_2-gas bubbling lasted for 3 and 7 h, respectively.

The surface OA-coating of all freshly oxidized precursors (PN1, PN2, POX1, POX3, and POX7) followed the same protocol,[26] namely, the wet solid sample (approximately 5 g) was initially suspended in 50 mL of distilled water, setting the medium at pH 8 using ammonium hydroxide aqueous solution (25%). Pure OA (50 mL) was then added to the suspension at room temperature under continuous stirring during 10 min. At the end of the stirring step, all the nanoparticulated material was transferred to the OA phase. The OA phase was isolated from the aqueous phase and washed three times with 80 mL of ethanol/acetone solution (2:1 v/v). The surface-coating step produced five different powder samples containing OA-coated maghemite nanoparticles labeled PN1OA, PN2OA, POX1OA, POX3OA, and POX7OA. Each OA-coated powder sample was split into two fractions and received different drying treatment. One fraction was dried at 40 °C under reduced pressure (RP) and used as powder samples in the material characterization steps. The second fraction was dried under N_2 stream (NS). The solid samples dried according to the NS route were dispersed in insulating mineral oil, producing insulating magnetic oils for transformer application and containing a 0.01% nanoparticle volume fraction. Accordingly, the prepared magnetic fluid samples (insulating magnetic oil) were labeled PNS-

Stability of Insulating Magnetic Oils

J. Phys. Chem. C, Vol. 114, No. 1, 2010 **181**

MF, PN1NS-MF, PN2NS-MF, POX1NS-MF, POX3NS-MF, and POX7NS-MF.

Sample Characterization Techniques. The Fe^{3+}/Fe^{2+} molar ratio in the as-prepared powder samples was obtained using the *o*-phenanthroline colorimetric method. XRD diffractograms of the powder samples were recorded in the 2θ range of $10-80°$ using the Shimadzu XRD-6000 system equipped with a Cu Kα radiation source. The diffractograms were used to check the phase of the SPIO-based material as well as to estimate the average crystallite size, the latter accomplished using the Scherrer equation.[41] The XRD data were refined using the PowderX software,[42] whereas the cell parameter was calculated using the Unitcell software applied to the measured peak positions of all major reflections in the range of $10-80°$ (2θ). Transmission electron microscopy (TEM) images were obtained using the JEOL-1011 microscope at 80 keV. The FT-IR measurements were carried out with samples dispersed in KBr (1%) and using the Bomem MB 100 spectrometer equipped with a DRIFT collector accessory, using the system's resolution set at 4 cm^{-1} while performing 128 scans. Thermogravimetric analyses (TG) were carried out in the Shimadzu DTG 60 system. Samples (5−6 mg) were analyzed from room temperature up to 1000 °C under 50 mL min^{-1} N$_2$ flow, using three different heating rates: 10 °C min^{-1} from room temperature up to 100 °C, 5 °C min^{-1} from 100 up to 600 °C, and 20 °C min^{-1} from 600 up to 1000 °C. All measurements were performed a few days after preparation of the samples. The hydrodynamic radius of the OA-coated maghemite nanoparticles dispersed in mineral oil was obtained by dynamic light scattering measurements using the Malvern Instrument Zeta Sizer Nano ZS90. The measurements were carried out using freshly prepared diluted dispersions. The colloidal stability of the insulating magnetic oils was monitored at room temperature in the time window of 24 months after preparation, by measuring the hydrodynamic radius and using visual inspection. The Raman system used to record the spectra of the powder samples was the Jobin Yvon T64000 equipped with a liquid-nitrogen-cooled CCD detector while the samples were excited using an argon ion laser ($\lambda = 514$ nm). The Raman measurements were performed at room temperature while controlling the laser intensity in the range of $0.5-16.1$ mW. Magnetization measurements (field- and temperature-dependent) of the native powder samples (P, PN2, POX1, POX3, and POX7) and OA-coated samples (POA, PN2OA, POX1OA, POX3OA, and POX7OA) were conducted using a Quantum Design PPMS extraction magnetometer. Zero-field-cooled (ZFC) and field-cooled (FC) magnetization curves were recorded while warming up the samples previously cooled down under zero-field and non-zero-field conditions, respectively.

Results and Discussion

Analysis of the XRD patterns of all powder samples investigated revealed cubic spinel structure (*Fd3m*), in agreement with the protocols used to produce the SPIO-based materials. Figure 1 shows the XRD patterns of samples P, PN1, PN2, POX1, POX3, and POX7. The line broadening (fwhm) of the (311) X-ray diffraction peak provided the estimation of the average diameter (D_{XRD}) of the nanoparticulated materials. The obtained D_{XRD} values are shown in Table 1, which includes the lattice parameters and the Fe^{3+}/Fe^{2+} molar ratios. Samples PN1 and PN2, obtained from the HT treatment of sample P, show very low Fe^{2+} contents (approximately 1.5% of total iron) with lattice parameter values very close to bulk maghemite (0.834 nm).[43,44] Samples POX1, POX3, and POX7, obtained by time-controlled BO treatment of the as-precipitated black
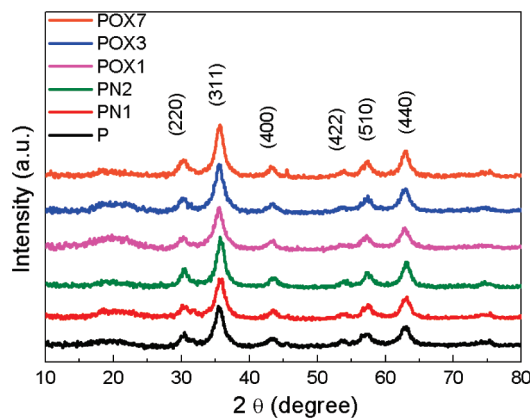
Figure 1. XRD patterns of samples P, PN1, PN2, POX1, POX3, and POX7.

precursor (sample P), revealed Fe^{2+} contents of 4.2, 2.5, and 1.6%, respectively. Note from Table 1 that the lattice parameters of samples POX1, POX3, and POX7 progressively approach the value quoted for bulk maghemite (0.834 nm) as the Fe^{2+} content reduces while increasing the BO treatment time. Furthermore, starting with the average nanoparticle size (D_{XRD}) of sample P, (5.7 nm) variation in this value was systematically observed in the data presented in Table 1. The XRD data show that both oxidation routes are successful in oxidizing nanosized magnetite to maghemite, though the HT treatment is much more effective than the BO treatment, given the conditions employed. In addition, both oxidation protocols increase the average particle size (D_{XRD}); the HT treatment increases the D_{XRD} as the concentration of the iron nitrate solution increases, whereas the BO treatment increases the D_{XRD} value as the treatment time increases. The increase in the average nanoparticle size via the HT treatment is more likely associated with a regrowth process taking place at the nanoparticle surface due to the availability of free ferric ions in solution. In contrast, the BO treatment does not add any extra iron ions into the reaction medium. Therefore, the more likely hypothesis regarding the observed increase in the average nanoparticle size as a consequence of the BO treatment is the mass transfer.[45] Because of the chemical conditions, the BO treatment dissolves the smallest particles while depositing the obtained aqueous iron ions at the surface of bigger particles.

Transmission electron microscopy (TEM) micrographs were recorded in order to access the sample's average particle size and size dispersity. Figure 2 shows the TEM image of sample POX3OA. The particle size histogram of sample POX3OA obtained from the TEM micrographs is shown in the inset of Figure 2, where vertical bars represent the experimental data, whereas the solid line results from the curve fitting of the data using the log-normal distribution function.[46] Values of the average particle diameter (D_{TEM}) and standard diameter deviation (σ) obtained from the fitting of the data presented in Figure 2 were 6.9 ± 0.2 nm and 0.28 ± 0.04, respectively. Note the relatively narrow characteristics of the particle size distribution and the bigger ($\approx$15% bigger) average particle diameter obtained from TEM (6.9 nm) compared with the average particle diameter obtained from XRD (5.9 nm). This finding supports the presence of a freshly deposited iron oxide layer, poorly crystallized, on top of the already existing bigger nanoparticles, in agreement with the hypothesis of the mass transfer mechanism claimed above and related to the BO treatment.

Figure 3 displays the IR spectra of the OA-coated samples in the $400-4000$ cm^{-1} range. The IR bands observed at 438,

TABLE 1: Compositional, Structural and Magnetic Data of Nanosized Magnetite and Nanosized Oxidized Magnetite Samples

sample	Fe^{3+}/Fe^{2+} molar ratio	D_{XRD} (nm)	lattice parameter (nm)	M_S (emu/g) at 4 K	T_B (K)
P	2.3	5.7	0.839	63	144
PN1	72	5.7	0.833		
PN2	66	6.7	0.833	62	138
POX1	23	5.8	0.839	49	128
POX3	40	5.9	0.837	60	120
POX7	62	6.6	0.836	60	140

583, and 636 cm^{-1} are attributed to the maghemite phase,[47] whereas IR absorptions due to the OA-coating peak at higher wavenumbers. The three IR structures attributed to the maghemite crystal lattice bands indicate a partially disordered γ-Fe$_3$O$_2$ phase,[48] in agreement with the picture discussed above of freshly deposited iron oxide at the surface as a result of both HT and BO treatments. The IR spectra of all samples investigated show bands in the 2750−3000 cm^{-1} region associated with the asymmetric and symmetric $\rangle$CH$_2$ and −CH$_3$ modes of the OA-saturated chain fragments. In addition, the =CH− mode of the OA-unsaturated chain fragment peaks at 3005 cm^{-1}. The IR

band peaking at 1717 cm^{-1} was attributed to the hydrogen-bonded carbonyl ($\rangle$C=O) stretching mode of the carboxylic group. The broad asymmetric (ν_a) and symmetric (ν_s) carboxylate (−COO$^-$) stretching modes appear in the 1360−1650 cm^{-1} region, where there is also a contribution of the δ-(−CH$_2$−) mode, occurring at 1464 cm^{-1}. The calculation of the wavenumber difference between both ν_a (−COO$^-$) at 1526 cm^{-1} and ν_s (−COO$^-$) at 1434 cm^{-1} suggests that the carboxylates are covalently bonded to the iron sites at the nanoparticle surface mainly by bidentate linkages.[49] However, shoulders at 1404 and 1365 cm^{-1} were observed in the right-hand side of the symmetric absorption band, indicating the presence of bridging linkages and/or ionic ammonium carboxylate groups.[50]

Figure 4 shows the TG curves of the OA-coated samples in the range of 25−1000 °C. In the range of 25−200 °C, the TG data indicated that all samples investigated show a mass loss from 3.7 up to 4.7%, mainly associated with the loss of adsorbed water. Once the IR data indicated the presence of residual ammonium carboxylates, the above-mentioned mass loss (from 25 to 200 °C) can also be partially due to the decomposition of this compound. Above 200 °C, the OA-coated samples developed three different TG profiles regarding the number of steps involving the oleic species. In the range of 200−430 °C, only one TG step was observed for samples POX3OA and PN1OA. However, two TG steps were observed for sample POX1OA; the first step occurring between 200 and 340 °C, whereas the second step appears in the range of 340−530 °C. Finally, samples POX7OA and PN2OA revealed three TG steps; the first one occurring between 200 and 430 °C, the second step developing in the range of 550−690 °C, and the third step extending up to 1000 °C.

Although the literature reports controversial interpretation associated with multiple events of mass loss observed in TG data of surface-coated magnetic nanoparticles,[51−53] in the case of long-chain carboxylates, many authors attribute the multiple events to the presence of a bilayer or quasi-bilayer configuration of molecular chains at the nanoparticle surface.[21,54,55] The high-temperature event is claimed to be due to the chemical bonding
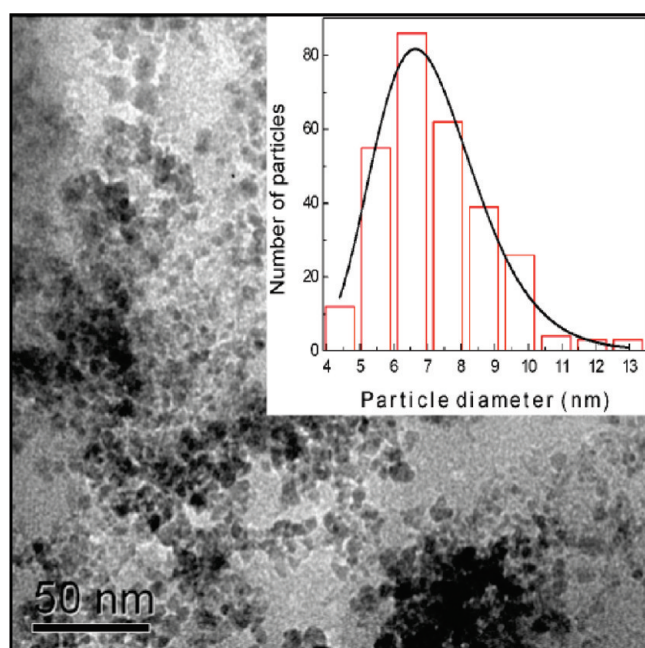
Figure 2. TEM micrograph of sample POX3OA. The inset shows the particle size histogram (vertical bars) of the sample. The solid line represents the best curve fitting using the log-normal distribution function.
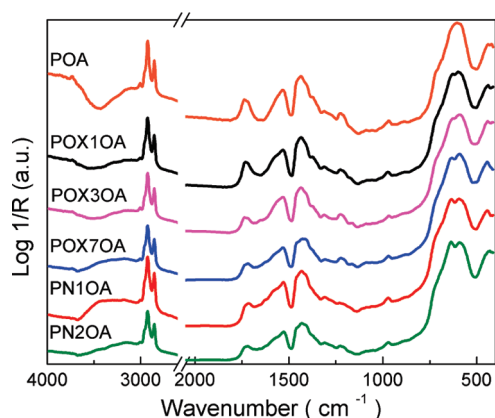
Figure 3. Infrared spectra for the OA-coated samples (POA, PN1OA, PN2OA, POX1OA, POX3OA, and POX7OA).
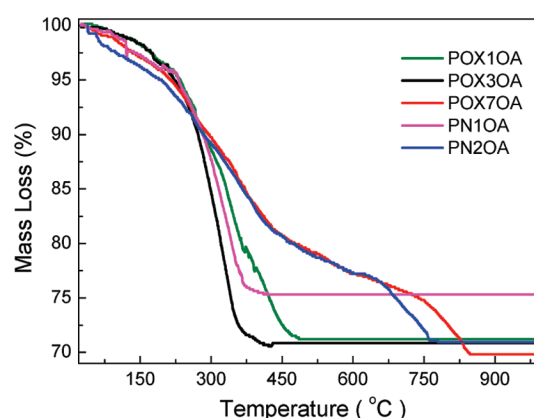
Figure 4. TG curves for the OA-coated samples (PN1OA, PN2OA, POX1OA, POX3OA, and POX7OA) performed under nitrogen flux.

Stability of Insulating Magnetic Oils

J. Phys. Chem. C, Vol. 114, No. 1, 2010 **183**

TABLE 2: TG Data of OA-Coated Magnetite and Oxidized Magnetite (Samples Quoted on the First Column) Include the Mass Loss Associated with Each Step Observed on the TG Curve and the Estimated Chemisorbed (ξ^C) and Physisorbed (ξ^P) Coefficients. The Saturation Magnetization at 4 K (M_S), the Blocking Temperature (T_B), and the Hydrodynamic Radius (R_H) of the Nanosized Particles Dispersed in Mineral Oil (Samples Quoted on the Last Column) Are Also Listed

| | mass loss (%) | | | grafting coefficients (nm^{-2})[a] | | | | | |
| | step 1 | step 2 | step 3 | | | | | | |
sample	200−430 °C	340−690 °C	550−1000 °C	ξ^C	ξ^P	M_S (emu/g)	T_B (K)	R_H (nm)	sample
POA	16.1	11.9		1.2	1.6	58	106	6.6	PNS-MF
PN1OA	20.9			2.1	nd			111.0	PN1NS-MF
PN2OA	13.4	4.5	5.8	0.8	1.6	69	118	11.8	PN2NS-MF
POX1OA	12.9	12.4		1.2	1.3	57	109	9.7	POX1NS-MF
POX3OA	25.7			2.6	nd	58	110	8.1	POX3NS-MF
POX7OA	14.3	5.1	10.6	0.9	1.6	64	116	11.9	POX7NS-MF

[a] nd: not detectable.

(chemisorption) of the carboxylate group to the surface Fe^{3+} ions, whereas the low-temperature event has been associated with physisorbed molecules inserted in between adjacent chemisorbed molecules.[54] Similar interpretation regarding the chemisorption and physisorption of long-chain carboxylates was employed by Capelle et al. in the study of adsorption of sodium stearate onto titania pigment.[56] Therefore, different TG profiles observed in the samples investigated here were rationalized considering different fractions of weakly bonded (physisorbed) and strongly bonded (chemisorbed) OA species. One single step of mass loss in the TG curve is expected when the chemisorbed OA species dominates. However, when a certain fraction of physisorbed OA species is present, the TG feature related to the chemisorbed OA species is retarded and at least two steps of mass loss are observed, the lower (higher)-temperature mass loss being attributed to the physisorbed (chemisorbed) OA species.[54] The above-mentioned retardation associated with the chemisorbed OA species while running the TG experiment can also cause polymerization of the remaining coating molecules, which may give rise to a third mass loss step at higher temperatures. The polymerization step at higher temperatures was suggested here because the DTA data (not shown) of samples PN2OA and POX7OA presented a continuous line with no distinguishable peaks.[57] The DTA curve of sample POX1OA reveals two exothermic peaks (320 and 415 °C), whereas only one single peak (300 °C) was observed for samples PN1OA and POX3OA.

Parameters obtained from the TG data are collected in Table 2, showing that the mass loss varied from 20.9 to 30.0%, sample POX7OA showing the highest content of OA species. The mass loss associated with samples POX1OA and POX3OA was similar (see Table 2), though the TG profiles are quite different, indicating that chemisorbed the OA species dominates in sample POX3OA (one single step), whereas sample POX1OA (two TG steps) may contain a considerable amount of physisorbed OA species in addition to the chemisorbed OA species. On the other hand, although sample POX7OA contains the highest total percentage of OA species, a lower fraction of chemisorbed OA species is present when compared with samples POX1OA and POX3OA. Likewise, while comparing samples PN1OA and PN2OA, one notices that the latter contains a higher total percentage of OA species, although it presents a lower fraction of chemisorbed OA species. The TG data indicate that the experimental condition employed in the oxidation of nanosized magnetite influences qualitatively and quantitatively the surface OA adsorption. Different from what has been reported in the literature,[58] Klokkenburg et al.[59] have noticed that the isotherms associated with the OA adsorption onto magnetite reached a plateau at a given coating species concentration, suggesting that

molecular adsorption is strongly dependent on the nanoparticle preparation route. Though the present study was not focused on the investigation of OA adsorption isotherms, it was possible to infer from our findings that different oxidation protocols produced nanosized maghemite particles bearing different surface reactivity. Indeed, it should be pointed out that, among the samples investigated, sample POX3OA presented the highest fraction of chemisorbed OA species. On the basis of the analysis of the TG curves, it was possible to calculate the average number of physisorbed and chemisorbed OA species onto the iron oxide nanoparticle surface using

$$OA/NP = \frac{P \times m_{NP}}{m_{OA} \times R} \quad (1)$$

where OA/NP is the number of OA species per nanoparticle, P is the mass loss of chemisorbed or physisorbed OA species obtained from the TG curve, m_{NP} is the nanoparticle mass (g) estimated using the density of bulk maghemite (5.49 g cm^{-3}) and the nanoparticle diameter (DRX data), m_{OA} is the OA molecule mass (g), and R is the mass of the final residue (Fe_2O_3) at the end of the TG experiment. While calculating OA/NP, the nanosized particles were considered perfectly spherical in shape. Further, the mass loss of physisorbed and chemisorbed OA species was obtained from the TG curves considering that the first step of mass loss was associated with OA molecules weakly bonded to the particle surface, whereas the subsequent steps were associated with strongly bonded OA molecules. Observation of one single step of mass loss (samples PN1OA and POX3OA) was associated with OA species strongly bonded onto the nanoparticle surface.

Average values of the surface grafting coefficient (ξ) for all samples investigated were obtained using

$$\xi = \frac{OA/NP}{A} \quad (2)$$

where OA/NP is the number of OA species (chemisorbed or physisorbed) per nanoparticle and A is the nanoparticle surface area calculated from the XRD data (particle diameter). Table 2 shows the chemisorbed (ξ^C) and physisorbed (ξ^P) grafting coefficients of the investigated samples. We found the total grafting coefficient ($\xi^C + \xi^P$) varied from 2.1 up to 2.6, the highest ξ^C value being associated with sample POX3OA. Theoretical calculation regarding the number of OA molecules per unit square at full monolayer coating onto magnetite particles gives around 3.8 molecules/nm^2, whereas values between 2.0 and 3.5 molecules/nm^2 have been obtained experimentally using mid-infrared spectroscopic measurements.[59] The grafting coefficients (ξ^C and ξ^P) estimated in the present study, based on

TG data, are quite useful to make comparison among our samples. Further, the grafting coefficients we found are in the same range of the values reported recently and based on TG measurements.[60] More interesting, we were able to correlate the values of the grafting coefficients (chemisorbed and physisorbed) with the colloidal stability of the prepared magnetic oils. The OA-coated nanoparticles were dispersed in mineral oil, and the hydrodynamic radii (R_H) were evaluated using dynamical light scattering (DLS) measurements (see R_H data in Table 2).
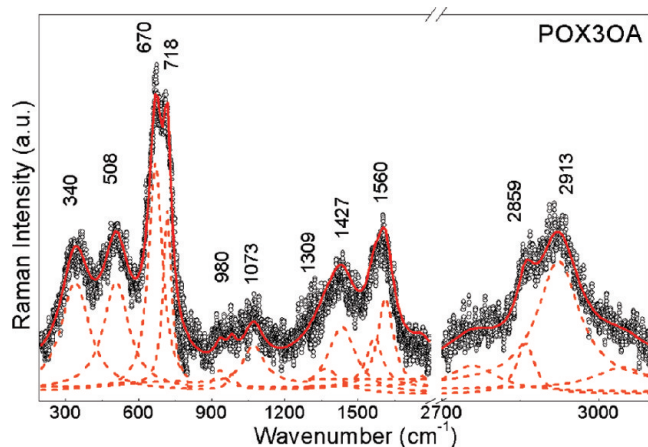
Atomic absorption measurements were used to obtain the iron content of 0.28, 0.30, 0.29, 0.27, 0.28, and 0.31 g L^{-1} for samples PNS-MF, PN1NS-MF, PN2NS-MF, POX1NS-MF, POX3NS-MF, and POX7NS-MF, respectively. All MF samples based on OA-coated nanosized particles suspended in mineral oil contained about 10^{15} particles/mL, meaning about a 0.01% nanoparticle volume fraction. The particle concentration (in units of particles/mL) and the nanoparticle volume fraction (in %) of all MF samples were calculated using the mass density of bulk maghemite and the nanoparticle diameter obtained from the XRD data. The freshly prepared MF samples presented R_H values in the range of 8.1−11.9 nm, except the MF sample produced from sample PN1OA with an R_H around 111.0 nm, which indicates particle aggregation. Particle aggregation attributed to sample PN1NS-MF may have occurred during the OA-coating procedure, possibly due to a particular surface characteristic of the nanosized particle at the pH of the reaction mixture. Not coincidentally, this sample showed the smaller grafting coefficient (2.1). We hypothesize that OA molecules were adsorbed at the surface of previously existing aggregates. Seven days after aging at room temperature, sample PN1NS-MF, produced from sample PN1OA, completely lost colloidal stability with formation of sediments, as shown in Figure 5. This trend was followed by MF samples presenting reduced values of chemisorbed OA species, namely, MF samples produced from POA, PN2OA, POX1OA, and POX7OA powders. After aging for 2 months samples PNS-MF, PN2NS-MF, POX1NS-MF, and POX7NS-MF lost colloidal stability with formation of sediments. The MF sample produced from POX3OA (POX3NS-MF) presented the highest colloidal stability, exhibiting no significant change in the R_H value nor any sedimentation in the time window of 24 months (see Figure 5). Therefore, excluding the presence of particle aggregation, as in the case of sample PN1NS-MF, the colloidal stability of the oil-based MF samples investigated in the present study increases with the amount of the chemisorbed OA species. Note that physisorbed species are usually desorbed out from the nanoparticle surface upon aging and/or dilution of the MF sample, reducing the steric repulsion among neighboring particles, thus leading to reduction of the colloidal stability. Furthermore, one might expect that, when the optimum amount (full monolayer) of chemisorbed molecules onto the nanoparticle surface is reached, any additional physisorbed molecules may contribute to reduce the colloidal stability.[58] Regarding the aspects presented above, MF samples produced from POX3OA revealed the highest chemisorbed (ξ^C) grafting coefficient, no detectable physisorbed (ξ^P) grafting coefficient, and the highest colloidal stability. Finally, our data indicated a strong correlation between colloidal stability and the Fe^{3+}/Fe^{2+} ratio (see Table 1) or, alternatively, the oxidation profile. Note from Table 1 that sample POX3 presents the Fe^{3+}/Fe^{2+} ratio around 40, whereas sample POX1 presents a lower Fe^{3+}/Fe^{2+} ratio (around 23), and samples PN1, PN2, and POX7 exhibit higher Fe^{3+}/Fe^{2+} ratios (from 62 to 72). In addition, note from Table 2 that sample POX3OA shows the highest chemisorbed grafting coefficient
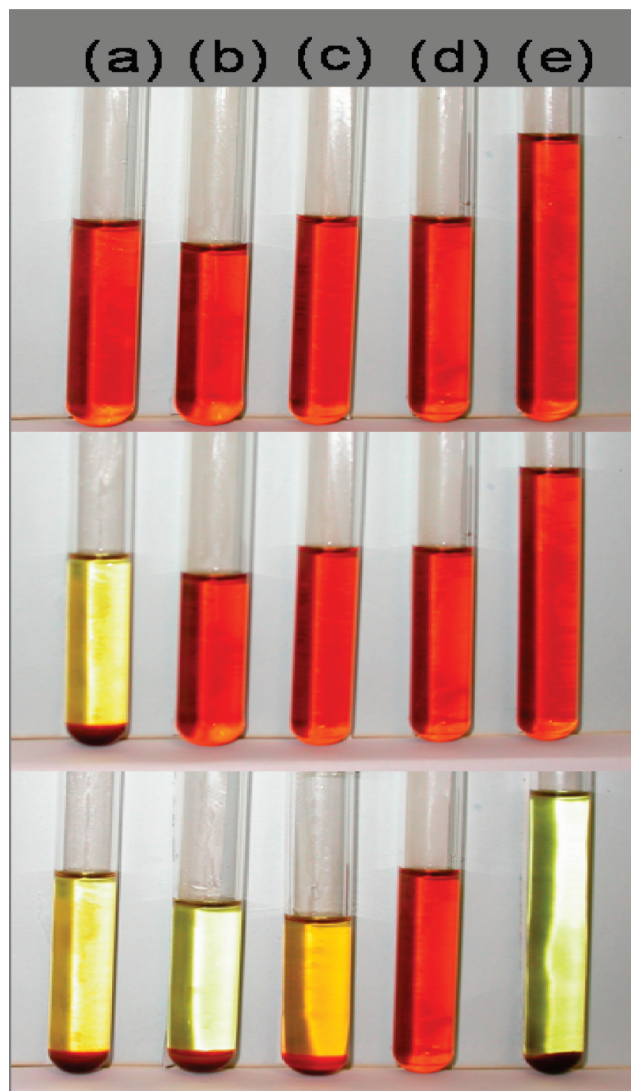
Figure 5. Pictures showing the MF samples' stability: PN1NS-MF (a), PN2NS-MF (b), POX1NS-MF (c), POX3NS-MF (d), and POX7NS-MF (e). Top images display the freshly prepared fluids, middle after seven days aging at room temperature, and bottom after 24 months. Note that only sample POX3NS-MF (d) remained stable (no sedimentation after 24 months).

(ξ^C) with no detectable physisorption, revealing the influence of the magnetite oxidation upon the surface OA adsorption. Considering that sample POX3NS-MF presented the highest colloidal stability, with no visible sedimentation after aging for 24 months, we claim that the OA-coated particles with Fe^{3+}/Fe^{2+} ratio values well above and well below 40 (2.5% of Fe^{2+} content) presented reduced colloidal stability in insulating mineral oil.

The Raman spectrum recorded using pure OA (provided in the Supporting Information) and the Raman spectrum of sample POX3OA (see Figure 6) were obtained at 0.5 mW laser excitation intensity. This laser intensity (0.5 mW) was used in order to avoid any possible sample degradation due to laser annealing.[61] The Raman spectrum of OA shows peaks at 1308, 1449, 2858, and 2902 cm^{-1}, attributed to the $-CH_2-$ twisting mode, $-CH_2-$ scissoring mode, and symmetric and asymmetric $-CH_2-$ stretching mode, respectively. Regarding the Supporting Information, Raman bands peaking at 1079 and 1661 cm^{-1} were assigned to C−C and C=C modes, respectively.[62] For sample POX3OA, the Raman features (see Figure 6) observed in the spectral region from 150 to 800 cm^{-1} were assigned to

Stability of Insulating Magnetic Oils

J. Phys. Chem. C, Vol. 114, No. 1, 2010 **185**

**Figure 6.** Room-temperature Raman spectrum recorded from sample POX3OA.

Figure 7. Room-temperature Raman spectra recorded for samples (a) POX1OA and (b) POX3OA using the laser excitation intensity set at (from bottom to top) 0.5, 1.6, 3.2, 6.4, and 16.1 mW.

vibrational modes from the iron-oxide-based structure (2 E_g, T_{2g}, and A_{1g}), whereas the band around 1400 cm^{-1} is characteristic of nanosized maghemite.[63−65] The fitting procedure applied to the Raman spectrum, using Lorentzian-like components, revealed the presence of structures at 340, 508, 670, 718, and 1427 cm^{-1}. Furthermore, the Raman bands observed at 980 and 1309 cm^{-1} (see Figure 6) can be attributed to −CH$_2$− modes associated with organic fragments of OA species, whereas Raman bands peaking at 1073 and 1560 cm^{-1} may suggest disordered carbon[66] and/or a mixture of ligands at the nanoparticle surface. Indeed, the Raman modes observed at 2859 and 2913 cm^{-1} can be attributed to symmetric and asymmetric −CH$_2$− stretching modes, as has been observed in the Raman spectrum of pure OA.

Raman measurements were also performed as a function of the laser excitation intensity (0.5−16.1 mW) for all investigated samples. At lower laser excitation intensities, the Raman spectra (not shown) of all uncoated samples (PN1, PN2, POX1, POX3, and POX7) revealed the characteristic bands of maghemite.[65] However, we found the onset of the hematite Raman peaks at the laser excitation intensity of 3.2 mW in all uncoated samples. This finding indicates that different oxidation treatments do not affect the uncoated samples' response under laser annealing. Likewise, Raman spectroscopy was used to investigate the OA-coated samples (PN1OA, PN2OA, POX1OA, POX3OA, and POX7OA) under different laser excitation intensities (0.5, 1.6, 3.2, 6.4, and 16.1 mW). The Raman spectra of samples POX1OA and POX3OA, recorded under different laser excitation intensities, are shown in Figure 7a,b, respectively. At this point, we should emphasize that samples POX1OA and POX3OA presented a similar total mass loss (see Table 2) but different decomposition profiles associated with the OA coating. Under 0.5 mW laser excitation intensity, the Raman features observed for both samples are quite similar, revealing the characteristic bands of maghemite in the lower (150−1400 cm^{-1}) spectral range and bands related to the OA coating in the higher (2800−3000 cm^{-1}) spectral range. However, the Raman spectrum of sample POX1OA recorded under 1.6 mW laser excitation intensity (see Figure 7a) reveals new features at 222 and 287 cm^{-1}. These new features (222 and 287 cm^{-1}) are characteristic Raman modes of hematite (α-Fe$_2$O$_3$), revealing the presence of both phases, maghemite and hematite, due to laser annealing. At the same laser excitation intensity (1.6 mW), the characteristic symmetric and asymmetric −CH$_2$− stretching modes peaking at 2859 and 2913 cm^{-1} disappear from the spectrum of sample POX1OA, while the intensity of the Raman
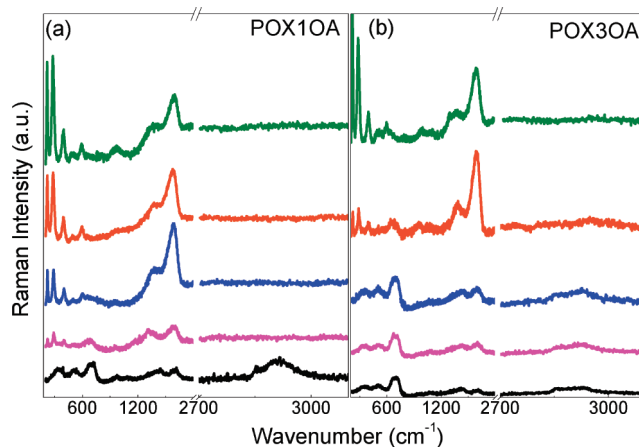
band attributed to disordered carbon (around 1600 cm^{-1}) increases. Differently, the Raman spectrum of sample POX3OA (Figure 7b) shows the onset of the hematite phase only at 6.4 mW laser excitation intensity. In addition, under 6.4 mW laser excitation intensity, the Raman spectrum of sample POX3OA still shows the characteristic OA-coating bands (−CH$_2$− stretching modes) in the higher (2800−3000 cm^{-1}) spectral range, while the disordered carbon band intensity (around 1600 cm^{-1}) increases. These findings can be understood on the basis of the amount of chemisorbed OA species at the nanoparticle surface. Once sample POX1OA presents a lower OA grafting coefficient (1.2 nm^{-2}) compared with sample POX3OA (2.6 nm^{-2}), the optically induced phase change from maghemite to hematite occurs at a lower laser excitation intensity. As far as the optically induced phase change threshold is concerned, the same trend was also observed in the Raman data of samples PN1OA and PN2OA. Whereas the characteristic hematite Raman peaks appear under 6.4 mW laser irradiation for sample PN1OA, the onset of the hematite Raman peaks for sample PN2OA occurs at 3.2 mW laser irradiation. These findings suggest that the nanoparticle structural stability against laser irradiation depends on the chemisorbed grafting coefficient; the higher the chemisorbed grafting coefficient the higher the phase stability against laser annealing.

Magnetic characteristics of all nanosized maghemite-based samples, uncoated and OA-coated, were evaluated using magnetic hysteresis loops and zero-field-cooled (ZFC)/field-cooled (FC) magnetization curves in a wide range of temperatures. Magnetic hysteresis loop measurements were performed at 4, 77, and 300 K, recording the data in the ± 20 kOe window. ZFC/FC magnetization curves (dc probing field set at 100 Oe) were recorded in the 4−300 K temperature range. Figures 8 and 9 show typical (sample POX3OA) hysteresis and ZFC/FC data, respectively. The inset in Figure 8 shows the details of the hysteresis loops of sample POX3OA in the ± 1 kOe window, at different temperatures. Note from the inset in Figure 8 that no remanence (M_R) or coercivity (H_C) were observed at 300 K, as one should expect from samples containing noninteracting nanosized (about 7 nm average diameter) maghemite particles. The saturation magnetization (M_S) was evaluated using the law of approach to saturation plotting the magnetization versus the reciprocal of the applied field.[67]

Low-temperature (4 K) $M \times H$ curves (data not shown) provided M_S values of 63, 62, 49, 60, and 60 emu/g for the surface-uncoated samples P, PN2, POX1, POX3, and POX7,
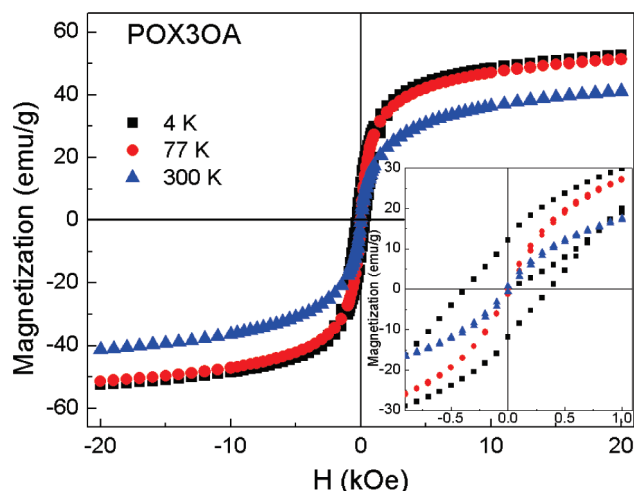
Figure 8. Magnetic hysteresis loops of sample POX3OA at different temperatures, as indicated. The inset shows the details of the $M \times H$ curves in a narrow window of field values.
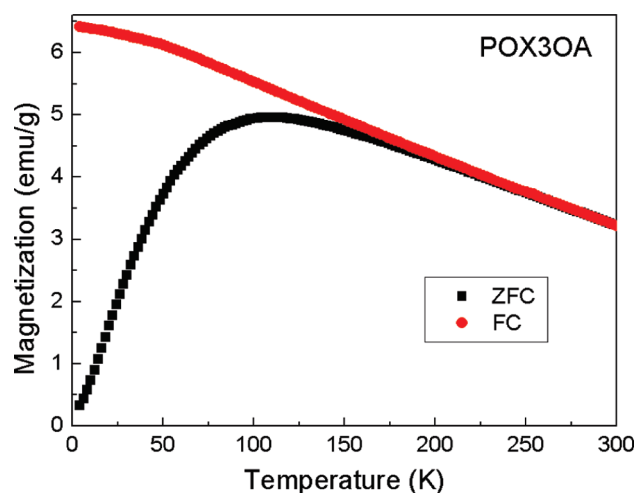
Figure 9. ZFC−FC curves of sample POX3OA recorded under 100 Oe dc applied field.

respectively. These values are smaller than the values reported for bulk maghemite at 4 K ($M_S = 85$ emug^{-1}). This finding is in agreement with the literature, describing the reduction of the saturation magnetization due to surface spin canting and disorder associated with broken bonds and frustration of exchange interactions.[68,69] The ZFC/FC curves (dc probing field at 100 Oe) of the surface-uncoated samples presented a blocking temperature (T_B) of 144, 138, 128, 120, and 140 K for samples P, PN2, POX1, POX3, and POX7, respectively. The data presented above indicate that M_S and T_B values scale to each other and are sensitive to both the average particle size and the Fe^{3+}/Fe^{2+} ratio, irrespective of the chemical route used to oxidize Fe^{2+} into Fe^{3+} (see data in Table 1). The same trends are found in the case of the OA-coated maghemite-based samples (see data in Table 2). The OA weight contribution has been subtracted to analyze the magnetization data of surface-coated maghemite-based samples. The observed saturation magnetizations of the OA-coated samples (POA, PN2OA, POX1OA, POX3OA, and POX7OA) obtained from the hysteresis loop at 4 K were 58, 69, 57, 58, and 64 emu/g. ZFC/FC magnetization curves of samples POA, PN2OA, POX1OA, POX3OA and POX7OA exhibit the typical blocking process of an assembly of superparamagnetic particles, with a blocking temperature around 106, 118, 109, 110, and 116 K, respectively.

Regarding the investigated powder samples, inspection of the data presented in Tables 1 and 2 shows a systematic reduction of T_B due to the OA coating. In comparison to the uncoated counterparts (P, PN2, POX1, POX3, and POX7), all the investigated OA-coated samples (POA, PN2OA, POX1OA, POX3OA, and POX7OA) displayed reduced T_B values. We claim that this is mainly due to the reduction of the particle−particle dipole interaction as the OA-coated particles are not allowed to be (in average) as close together as the uncoated counterparts. Observation of the systematic higher R_H values associated with the OA-coated samples compared with the R_{XRD} values observed in the uncoated ones (see data in Tables 1 and 2) supports our explanation. As quoted in Tables 1 and 2, we found from the magnetization measurements that the M_S value of the OA-coated precursor (POA) is lower than the M_S value of the uncoated precursor (P). This finding is in agreement with the data reported in the literature regarding the surface-coating of nanosized magnetite particles with carboxylate moieties.[70] It should be emphasized here that this finding could be the actual trend for nanosized iron oxide presenting stoichiometry very close to magnetite ($Fe^{3+}/Fe^{2+} \approx 2$). However, in all oxidized samples reported in this study ($Fe^{3+}/Fe^{2+} \gg 2$), the OA-coating enhances the M_S value as compared with the uncoated counterparts. This observation is in opposition to the finding related to the nanosized magnetite, in which case the OA-coating leads to reduction of the M_S value. This aspect deserves more deep investigation, though it seems to be related to the availability of Fe^{3+} at surface sites. The P sample (magnetite) presents both Fe^{3+} and Fe^{2+} at surface sites, whereas the oxidized samples present mostly Fe^{3+}. Carboxylate complexation of Fe^{3+} leads to more stable complexes than carboxylate complexation of Fe^{2+}, and this fact is likely to be related to our findings.[71,72] The stronger the surface iron sites complexation with carboxylate moieties the thinner one should expect the surface magnetic dead layer, resulting in the enhancement of the saturation magnetization. For uncoated as well as for OA-coated samples, the M_S values within the POX series increase as the Fe^{3+}/Fe^{2+} ratio increases (see data in Tables 1 and 2). The observed trend could be due to a combination of factors, among them the systematic increase of the average particle size, the improvement of the crystallinity due to the thermal treatment under oxygen stress, and the approach to the stoichiometry of pure maghemite, the latter supported by the evolution of the unit cell parameter.

Conclusions

Native magnetic iron oxide-based nanoparticulated materials with an average diameter around 6 nm and presenting stoichiometry very close to maghemite were produced via oxidation of a freshly precipitated magnetite sample. Two different routes of oxidation of nanosized magnetite were employed in the present study, each one using progressive oxidative stress, resulting in five different native iron oxide nanoparticulated samples. All native iron oxide samples were surface-functionalized using oleic acid, suspended in insulating mineral oil and evaluated in terms of their colloidal stability. Thermogravimetric analysis of the surface-functionalized samples indicated the strong influence of the oxidation protocol upon the oleic acid anchoring at the nanoparticle surface, as indicated by the relative content of physisorbed and chemisorbed species. We found the smallest hydrodynamic diameter and the highest colloidal stability associated with the suspension containing oleic acid chemisorbed (exclusively) onto iron oxide nanoparticles. The highest colloidal stability was observed for the surface-functionalized nanoparticle produced via bubbling oxygen gas

Stability of Insulating Magnetic Oils

J. Phys. Chem. C, Vol. 114, No. 1, 2010 **187**

through an acidic suspension of the as-precipitated magnetite, leading to $Fe^{3+}/Fe^{2+} = 40$ (2.5% of Fe^{2+} content). Besides the best colloidal stability provided by the highest content of oleic acid chemisorption, the core iron oxide presented the highest stability against phase change to hematite induced by laser annealing. We found the oxidation of magnetite via bubbling oxygen gas through its acidic suspension more appropriate for modulating the characteristics of the end product, including the Fe^{3+}/Fe^{2+} ratio, particle size, and lattice constant, as quoted in Table 1. Despite the oxidation process and, therefore, the details of the end product, we found a systematic reduction of the blocking temperature due to the oleic acid coating, here mainly attributed to the reduction of the dipole−dipole interaction. Finally, we found the enhancement of the saturation magnetization associated with the carboxylate complexation of the Fe^{3+}-rich terminated surface in iron oxide nanoparticles as opposed to Fe^{3+}/Fe^{2+}-terminated surfaces, as in the case of magnetite. This finding is claimed to be mostly related to the enhancement of the superexchange interaction taking place at the terminated surface due to the higher strength of the Fe^{3+}−carboxylate complex in comparison with the strength of Fe^{2+}−carboxylate complex, leading to the reduction of the effective magnetic dead layer thickness.

Supporting Information Available: Raman spectrum recorded using pure oleic acid (Figure 1S). This material is available free of charge via the Internet at http://pubs.acs.org.

References and Notes

(1) Segal, V.; Rabinovicj, A.; Nattrass, D.; Raj, K.; Nunes, A. *J. Magn. Magn. Mater.* **2000**, *215−216*, 513.

(2) Sartoratto, P. P. C.; Neto, A. V. S.; Lima, E. C. D.; Rodrigues de Sá, A. L. C.; Morais, P. C. *J. Appl. Phys.* **2005**, *97*, 10Q917.

(3) Kopčanský, P.; Toměo, L.; Marton, K.; Koneracká, M.; Timko, M.; Potočová, I. *J. Magn. Magn. Mater.* **2005**, *289*, 415.

(4) Cunha, F. R.; Couto, H. L. G.; Marcelino, N. B. *Magnetohydrodynamics* **2007**, *43*, 421.

(5) Islam, T.; Josephson, L. *Cancer Biomarkers* **2009**, *5*, 99.

(6) Kodama, R. H. *J. Magn. Magn. Mater.* **1999**, *200*, 359.

(7) Batlle, X.; Labarta, A. *J. Phys. D: Appl. Phys.* **2002**, *35*, R15.

(8) Liao, W.; Chen, X.; Chen, Y.; Pu, S.; Xia, Y.; Li, Q. *Appl. Phys. Lett.* **2005**, *87*, 151122.

(9) Magnani, M.; Galluzzi, L.; Bruce, I. J. *J. Nanosci. Nanotechnol.* **2006**, *6*, 9.

(10) Babič, M.; Horák, D.; Trchová, M.; Jendelová, P.; Glogarová, K.; Lesný, P.; Herynek, V.; Hájek, M.; Syková, E. *Bioconjugate Chem.* **2008**, *19*, 740.

(11) Valdés-Solís, T.; Rebolledo, A. F.; Sevilla, M.; Valle-Vigon, P.; Bomatí-Miguel, O.; Fuertes, A. B.; Tartaj, P. *Chem. Mater.* **2009**, *21*, 1806.

(12) Guo, Q.; Teng, X.; Rahman, S.; Yang, H. *J. Am. Chem. Soc.* **2003**, *125*, 630.

(13) Pedroza, R. C.; da Silva, S. W.; Soler, M. A. G.; Sartoratto, P. P. C.; Rezende, D. R.; Morais, P. C. *J. Magn. Magn. Mater.* **2005**, *289*, 139.

(14) Grigoriev, D.; Gorin, D.; Sukhorukov, G. B.; Yashchenok, A.; Maltseva, E.; Möhwald, H. *Langmuir* **2007**, *23*, 12396.

(15) Paterno, L. G.; Soler, M. A. G.; Fonseca, F. J.; Sinnecker, J. P.; Sinnecker, E. H. C. P.; Lima, E. C. D.; Novak, M. A.; Morais, P. C. *J. Phys. Chem. C* **2009**, *113*, 5087.

(16) Rosensweig, R. E. *Ferrohydrodynamics*; Cambridge University Press: Cambridge, U.K., 1985.

(17) Blums, E.; Cebers, A.; Mairov, M. M. *Magnetic Fluids*; Walter de Guyter: Berlin, 1985.

(18) Hyeon, T.; Lee, S. S.; Park, J.; Chung, Y.; Na, H. B. *J. Am. Chem. Soc.* **2001**, *123*, 12798.

(19) Willis, A. L.; Turro, N. J.; O'Brien, S. *Chem. Mater.* **2005**, *17*, 5970.

(20) Pascal, C.; Pascal, J. L.; Favier, F.; Elidrissi Moubtassim, M. L.; Payen, C. *Chem. Mater.* **1999**, *11*, 141.

(21) Sahoo, Y.; Pizem, H.; Fried, T.; Golodnitsky, D.; Burstein, L.; Sukenik, C. N.; Markovich, G. *Langmuir* **2001**, *17*, 7907.

(22) Tartaj, P.; Morales, M. P.; Veintemillas-Verdaguer, S.; Gonzázels-Carreño, T.; Serna, C. J. *J. Phys. D: Appl. Phys.* **2003**, *36*, R182.

(23) Sun, X.; Zheng, C.; Zhang, F.; Li, L.; Yang, Y.; Wu, G.; Guan, N. *J. Phys. Chem. C* **2008**, *112*, 17148.

(24) Tourinho, F. A.; Franck, R.; Massart, R. *J. Mater. Sci.* **1990**, *25*, 3249.

(25) Kang, Y. S.; Risbud, S.; Rabolt, J. F.; Stroeve, P. *Chem. Mater.* **1996**, *8*, 2209.

(26) van Ewijk, G. A.; Vroege, F. J.; Philipse, A. P. *J. Magn. Magn. Mater.* **1999**, *201*, 31.

(27) Morais, P. C.; Garg, V. K.; Oliveira, A. C.; Silva, L. P.; Azevedo, R. B.; Silva, A. M. L.; Lima, E. C. D. *J. Magn. Magn. Mater.* **2001**, *225*, 37.

(28) Jolivet, J. P.; Belleville, P.; Tronc, E.; Livage, J. *Clays Clay Miner.* **1992**, *40*, 531.

(29) Gnanaprakash, G.; Philip, J.; Jayakumar, T.; Raj, B. *J. Phys. Chem. B* **2007**, *111*, 7978.

(30) Segal, V.; Raj, K. *Indian J. Eng. Mater. Sci.* **1998**, *5*, 416.

(31) Segal, V.; Hjortsberg, A.; Rabinovich, A.; Nattrass, D.; Raj, K. *Conference Record of the IEEE International Symposium on Electrical Insulation*, Arlington, Virginia, 1998; p 619.

(32) Segal, V. Colloidal insulating and cooling fluid - composed of carrier liquid and non-metallic particles. U.S. Patent 5,863,455, January 26, 1999.

(33) Tomco, L.; Kopcansky, P.; Tomasovicova, N.; Koneracka, M.; Timko, M. *Czech. J. Phys.* **2002**, *52*, A285.

(34) Kopcansky, P.; Tomco, L.; Marton, K.; Koneracka, M.; Potocova, I.; Timko, M.; Jadzyn, J.; Czechowski, G. *Phys. Status Solidi B* **2003**, *236*, 454.

(35) Patel, R.; Parekh, K.; Upadhyay, R. V.; Mehta, R. V. *Indian J. Eng. Mater. Sci.* **2004**, *11*, 301.

(36) Kopcansky, P.; Koneracka, M.; Timko, M.; Potocova, I.; Marton, K.; Tomco, L. *Czech. J. Phys.* **2004**, *54*, D659.

(37) Parekh, K.; Upadhyay, R. V. *Indian J. Eng. Mater. Sci.* **2004**, *11*, 262.

(38) Kopcansky, P.; Tomco, L.; Marton, K.; Koneracka, M.; Potocova, I.; Timko, M. *J. Magn. Magn. Mater.* **2004**, *272−276*, 2377.

(39) Herchl, F.; Marton, K.; Tomco, L.; Kopcansky, P.; Timko, M.; Koneracka, M.; Kolcunova, I. *J. Phys.: Condens. Matter* **2008**, *20*, 204110.

(40) Herchl, F.; Kopcansky, P.; Timko, M.; Koneracka, M.; Marton, K.; Kolcunova, I.; Tomco, L. *Acta Phys. Pol., A* **2008**, *113*, 569.

(41) Cullity, B. D. *Elements of X-ray Diffraction*; Addison-Wesley: Reading, MA, 1978; p 101.

(42) Dong, C.; Chen, H.; Wu, F. *J. Appl. Crystallogr.* **1999**, *32*, 168.

(43) Krupicka, S.; Novak, P. *Oxide Spinels*; North-Holland Physics Publishing: Amsterdam, 1982; Vol. 3, p 192.

(44) International Center for Diffraction Data, PDF Card 22-1086, 2000.

(45) Morais, P. C.; Skeff Neto, K. *Polyhedron* **1983**, *2*, 875.

(46) Popplewell, J.; Sakhnini, L. *J. Magn. Magn. Mater.* **1995**, *149*, 72.

(47) Jing, Z.; Wu, S. *J. Solid State Chem.* **2004**, *177*, 1213.

(48) Morales, M. P.; Veintemillas-Verdaguer, S.; Montero, M. I.; Serna, C. J.; Roig, A.; Casas, L.; Martinez, B.; Sandiumenge, F. *Chem. Mater.* **1999**, *11*, 3058.

(49) Kirwan, L. J.; Fawell, P. D.; van Bronswijk, W. *Langmuir* **2004**, *20*, 4093.

(50) Nakamoto, K. *Infrared and Raman Spectra of Inorganic and Coordination Compounds*, 5th ed.; Wiley: New York, 1986.

(51) Zhang, L.; He, R.; Gu, H.-C. *Appl. Surf. Sci.* **2006**, *253*, 2611.

(52) Payman, R.; Holmgren, A. *Appl. Surf. Sci.* **2009**, *255*, 5891.

(53) Ayyappan, S.; Gnanaprakash, G.; Panneerselvam, G.; Antony, M. P.; Philip, J. *J. Phys. Chem. C* **2008**, *112*, 18376.

(54) Zboril, R.; Bakandritsos, A.; Mashlan, M.; Tzitzios, V.; Dallas, P.; Trapalis, Ch.; Petridis, D. *Nanotechnology* **2008**, *19*, 095602.

(55) Shen, L. F.; Laibinis, P. E.; Hatton, T. A. *Langmuir* **1999**, *15*, 447.

(56) Capelle, H. A.; Britcher, L. G.; Morris, G. E. *J. Colloid Interface Sci.* **2003**, *268*, 293.

(57) Dhoke, S. K.; Palraj, S.; Maruthan, K.; Selvaraj, M. *Prog. Org. Coat.* **2007**, *59*, 21.

(58) Dubois, E.; Cabuil, V.; Boue, F.; Perzynski, R. *J. Chem. Phys.* **1999**, *111*, 7147.

(59) Klokkenburg, M.; Hilhorst, J.; Erne, B. H. *Vib. Spectrosc.* **2007**, *43*, 243.

(60) Payman, R.; Holmgren, A. *Appl. Surf. Sci.* **2009**, *255*, 5891.

(61) Silva, S. W.; Melo, T. F. O.; Soler, M. A. G.; Lima, E. C. D.; Da Silva, M. F.; Morais, P. C. *IEEE Trans. Magn.* **2003**, *39*, 26.

(62) Soderlind, F.; Pedersen, H.; Petoral, R. M.; Kall, P.-O.; Uvdal, K. *J. Colloid Interface Sci.* **2005**, *288*, 140.

(63) de Faria, D. L. A.; Venâncio Silva, S.; de Oliveira, M. T. *J. Raman Spectrosc.* **1997**, *28*, 873.

(64) Chourpa, I.; Douziech-Eyrolles, L.; Ngaboni-Okassa, L.; Fouquenet, J.; Cohen-Jonathan, S.; Soucé, M.; Dubois, P. *Analyst* **2005**, *130*, 1395.

(65) Soler, M. A. G.; Alcantara, G. B.; Soares, F. Q.; Viali, W. R.; Sartoratto, P. P. C.; Fernandez, J. R. L.; Da Silva, S. W.; Garg, V. K.; Oliveira, A. C.; Morais, P. C. *Surf. Sci.* **2007**, *601*, 3921.

(66) Ferrari, A. C.; Robertson, J. *Phys. Rev. B* **2000**, *61*, 14095.

(67) Franklin, A. D.; Berkowitz, A. E. *Phys. Rev.* **1953**, *89*, 1171.

(68) Shafi, K. V. P. M.; Gedanken, A.; Prozorov, R.; Balogh, J. *Chem. Mater.* **1998**, *10*, 3445.

(69) Tung, L. D.; Kolesnichendo, V.; Caruntu, D.; Chou, N. H.; O'Connor, C. J.; Spinu, L. *J. Appl. Phys.* **2003**, *93*, 7486.

(70) Daou, T. J.; Grenèche, J. M.; Pourroy, G.; Buathong, S.; Derory, A.; Ulhaq-Bouillet, C.; Donnio, B.; Guillon, D.; Begin-Colin, S. *Chem. Mater.* **2008**, *20*, 5869.

(71) Cotton, F. A.; Wilkinson, G.; Murillo, C. A.; Bochmann, M.; Grimes, R. *Advanced Inorganic Chemistry*, 6th ed.; Wiley: New York, 1999.

(72) Ramadan, A. A. T.; El-Behairy, M. A.; Ismail, A. I.; Mahmoud, M. M. *Monatsh. Chem.* **1994**, *125*, 1171.